Supplementary Materials for

Suppression of radiation-induced hardening in intermetallic dispersion-strengthened ferritic superalloys

Kan Ma *et al.*

*Corresponding author. Kan Ma, email: kan.ma@cityu.edu.hk, Alexander Knowles, email: a.j.knowles@bham.ac.uk.

Table S 1 Composition of FNAT-Fine and FNAT-Coarse by SEM-EDS

Materials	Nominal (at.%)				SEM-EDS composition (at.%)			
	Al	Ti	Ni	Fe	Al	Ti	Ni	Fe
FNAT-Fine	13.5	13.5	20	53	12.0±0.2	14.4±0.1	19.9±0.1	53.7±0.2
FNAT-Coarse	13.5	13.5	20	53	12.1±0.1	14.5±0.1	19.9±0.1	53.4±0.2

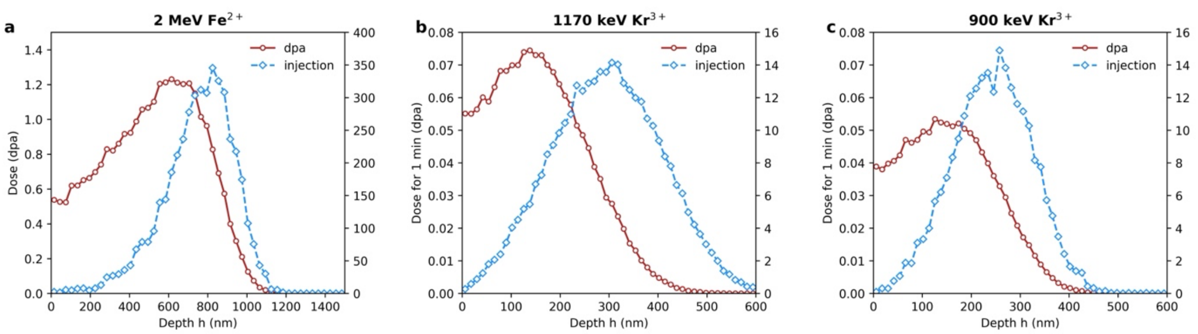

Fig. S1 Profiles of damage (in dpa) and implantation (in appm) calculated by SRIM. In (b) and (c) the dose is plotted for 1 min to indicate the dose rate of in-situ irradiation.

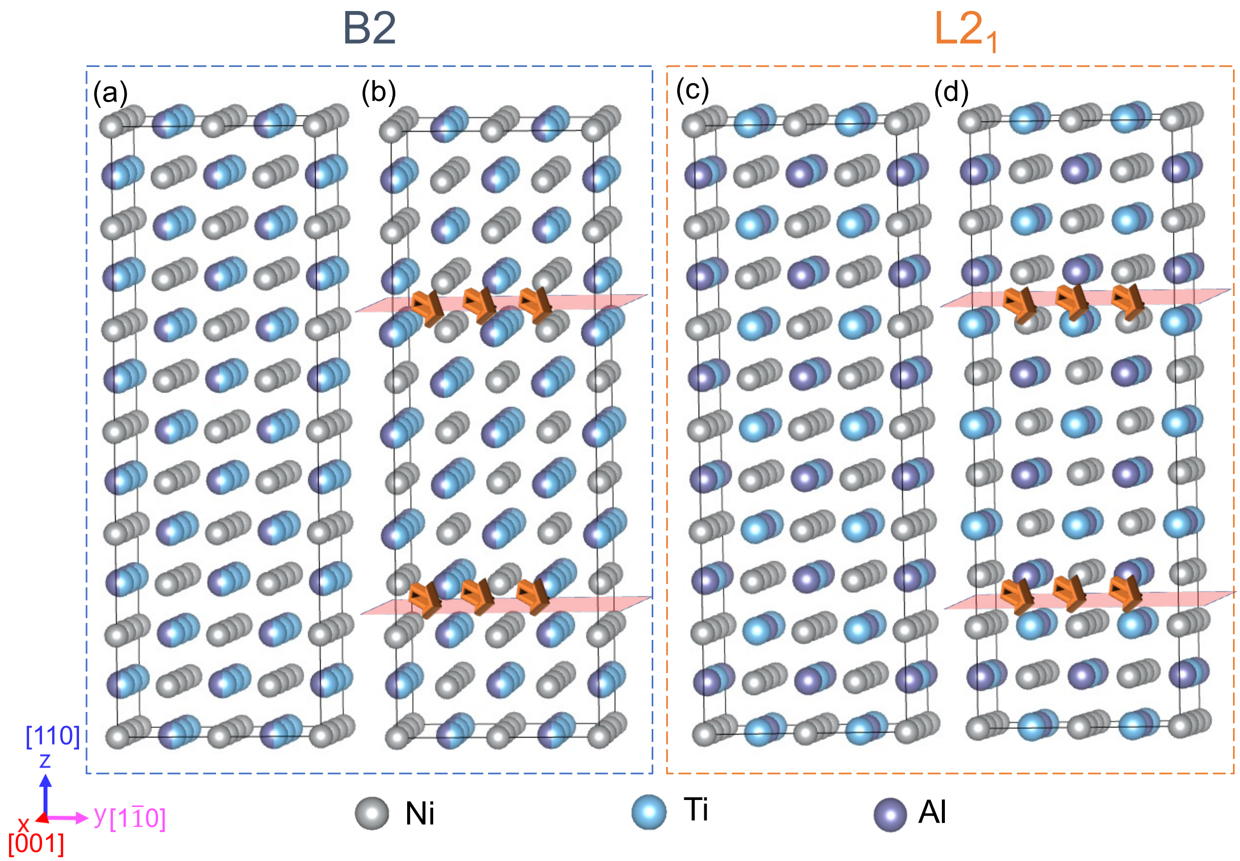

Fig. S2 Atomic configurations of B2 and $L2_1$ structures: (a) Pristine B2 structure; (b) APB configuration in B2 structure created by applying a shear displacement vector of $\frac{1}{2}[1\bar{1}1]$ (red arrows) along the {110} plane; (c) Pristine $L2_1$ structure; (d) APB configuration in $L2_1$ structure generated by applying a shear displacement vector of $\frac{1}{2}[1\bar{1}1]$ (red arrows) along the {110} plane.

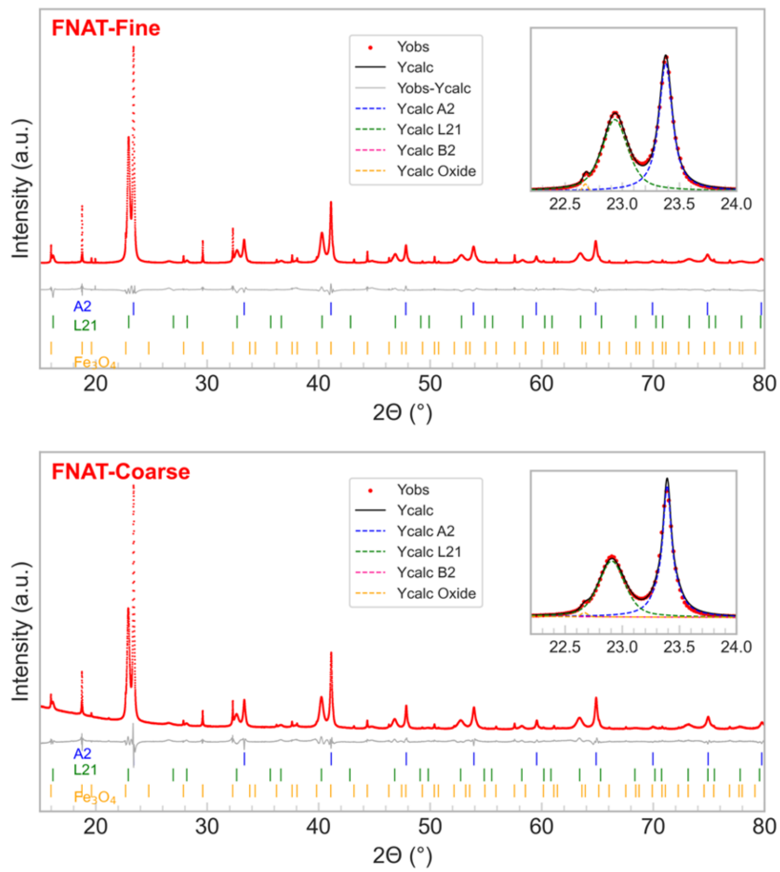

Fig. S3 Synchrotron X-ray diffraction (SXRD) of FNAT-Fine and FNAT-Coarse alloys. SXRD spectrums are refined using the Fullprof suite software with the A2 structure, L21 structure and Fe2O3 structure.

Table S 2 Lattice parameters and misfit in FNAT-Fine and FNAT-Coarse.

sample	Lattice parameter (Å)		Misfit
	$L2_1$	A2	(%)
FNAT-Fine	5.8701 ± 0.001	2.8800 ± 0.001	+1.89
FNAT-Coarse	5.8771 ± 0.001	2.8785 ± 0.001	+2.06
Eurofer97	/	2.868 ± 0.001	/

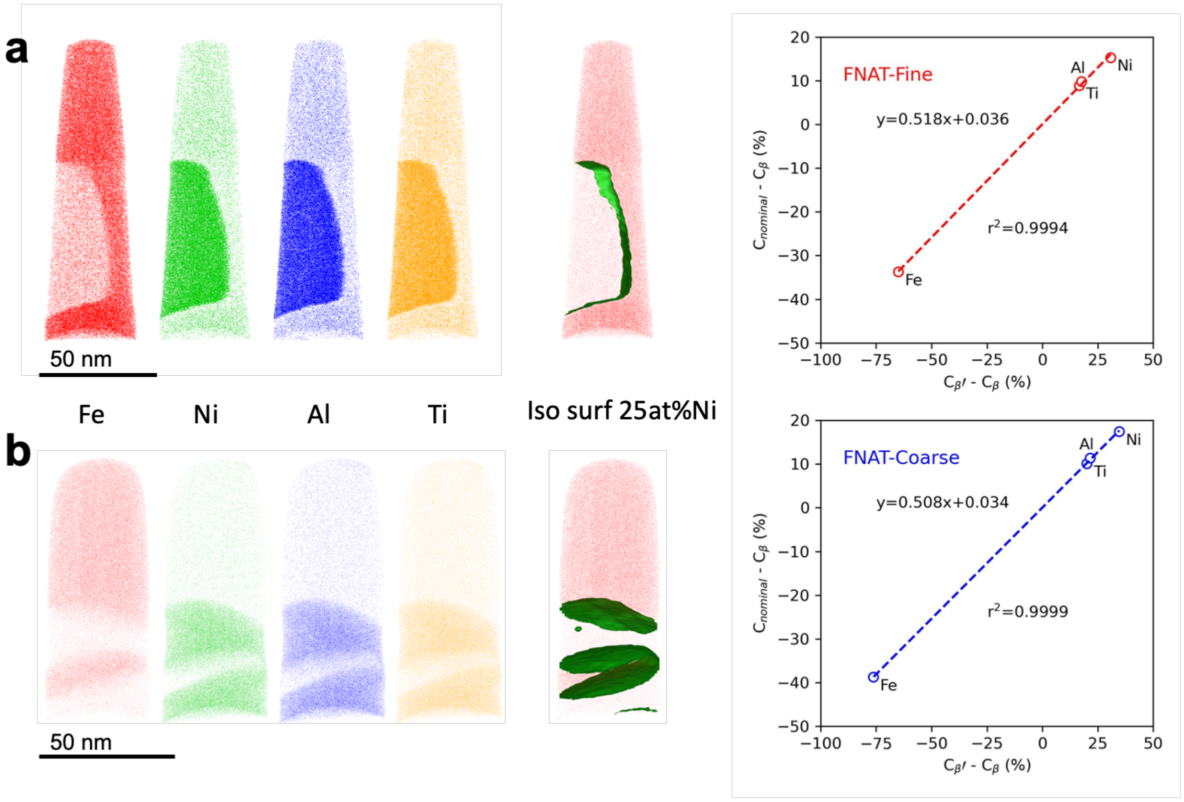

Fig. S4 Element maps of unirradiated (a) FNAT-Fine and (b) FNAT-Coarse with the plot of Lever rule to determine the volume fraction of precipitates.

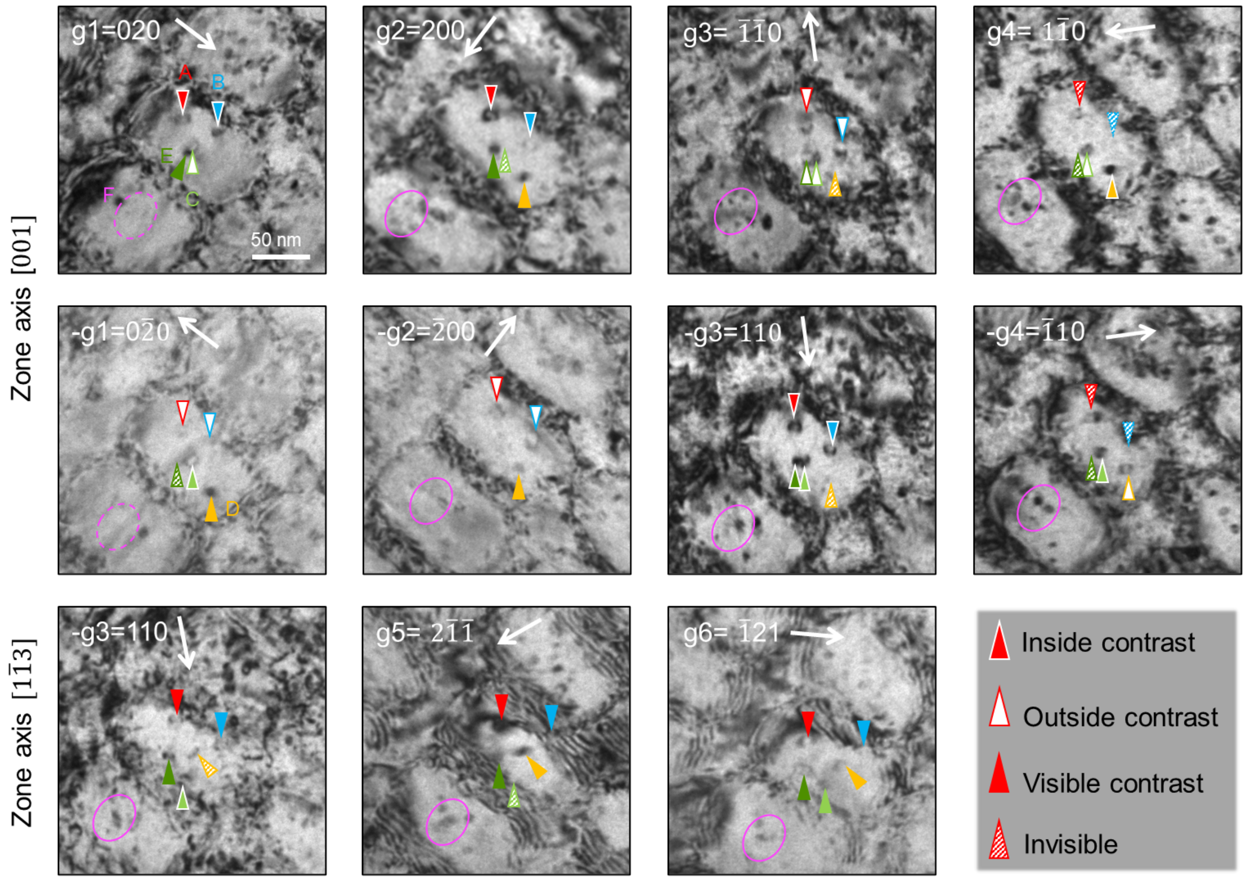

Fig. S5 Contrast of dislocation loops within precipitates in the irradiated FNAT-Fine alloy.

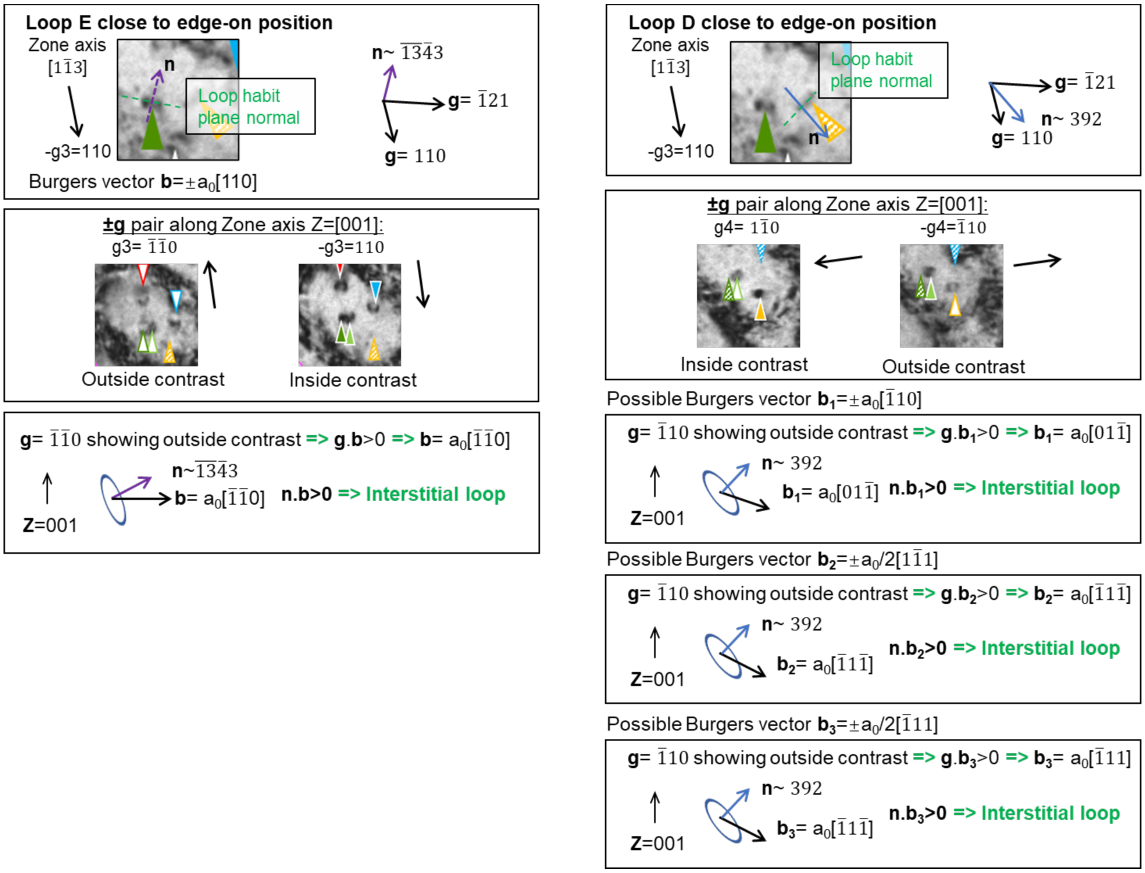

Fig. S6 Loop nature analysis in FNAT-Fine alloy.

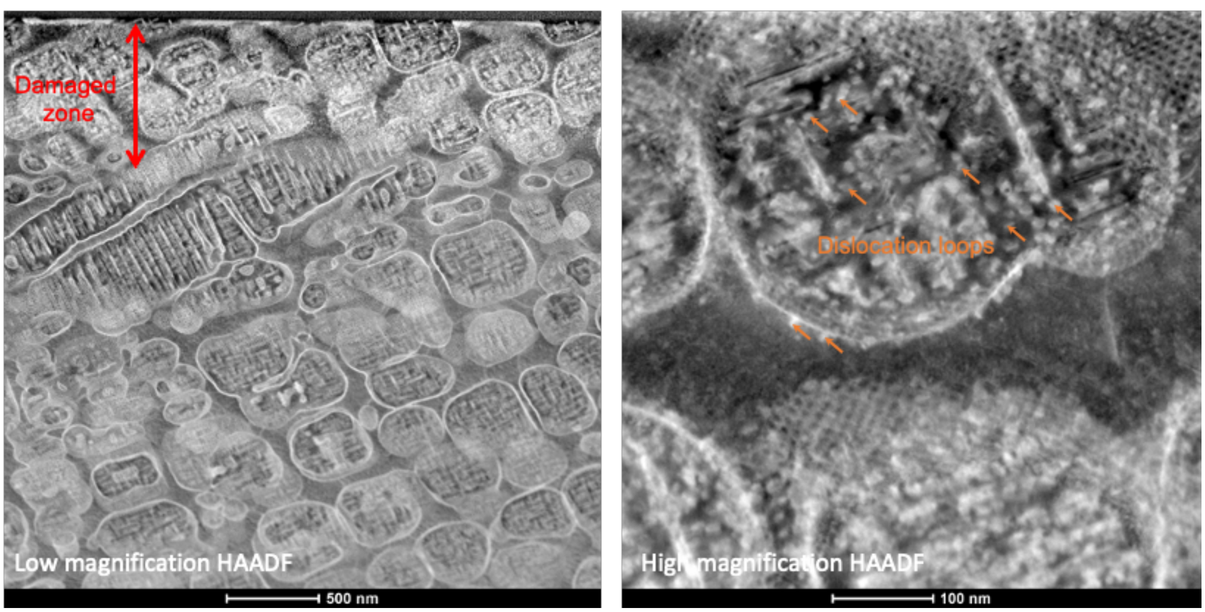

Fig. S7 STEM micrograph of irradiated FNAT-Coarse showing the formation of dislocation loops inside and at vicinity of precipitates.

Table S3. Visibility table of dislocation loops in FNAT-Fine to identify the Burgers vectors.

Burgers vectors	g1=020	g2=200	g3=-1-10	g4=1-10	g5=2-1-1	g6=-121	Loops
[100]	I	V	V	V	V	V	
[010]	V	I	V	V	V	V	
[001]	I	I	I	I	V	V	
1/2[111]	V	V	V	I	I	V	B?
1/2[-111]	V	V	I	V	V	V	D?
1/2[1-11]	V	V	I	V	V	V	D?
1/2[-1-11]	V	V	V	I	V	I	B?
[110]	V	V	V	I	V	V	A, E, B?
[1-10]	V	V	I	V	V	V	D?
[101]	I	V	V	V	V	I	
[-101]	I	V	V	V	V	V	F
[011]	V	I	V	V	V	V	
[0-11]	V	I	V	V	I	V	C

V: visible. I: invisible.

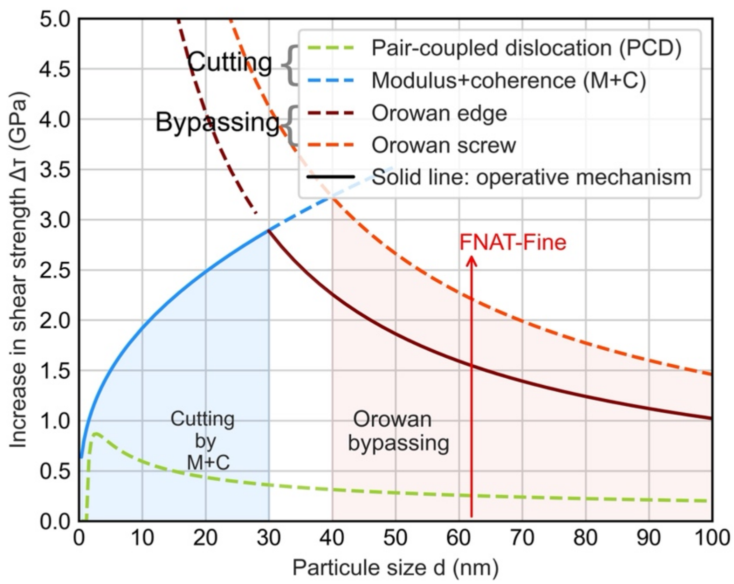

Fig. S8 Strengthening mechanism analysis in FNAT alloy.

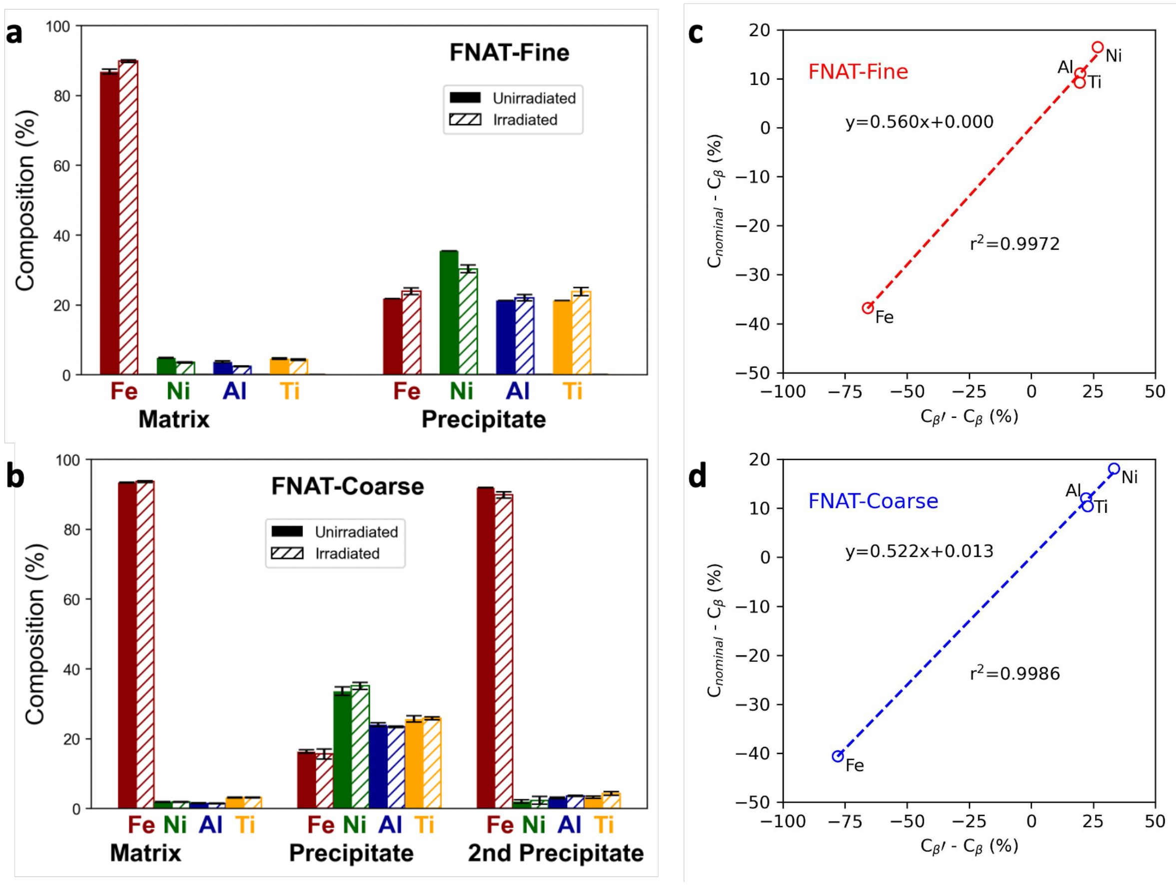

Fig. S9 Composition of the matrix, precipitates and secondary precipitates by APT in irradiated (a) FNAT-Fine and (c) FNAT-Coarse with (c,d) corresponding volume fraction analysis using Lever rule.

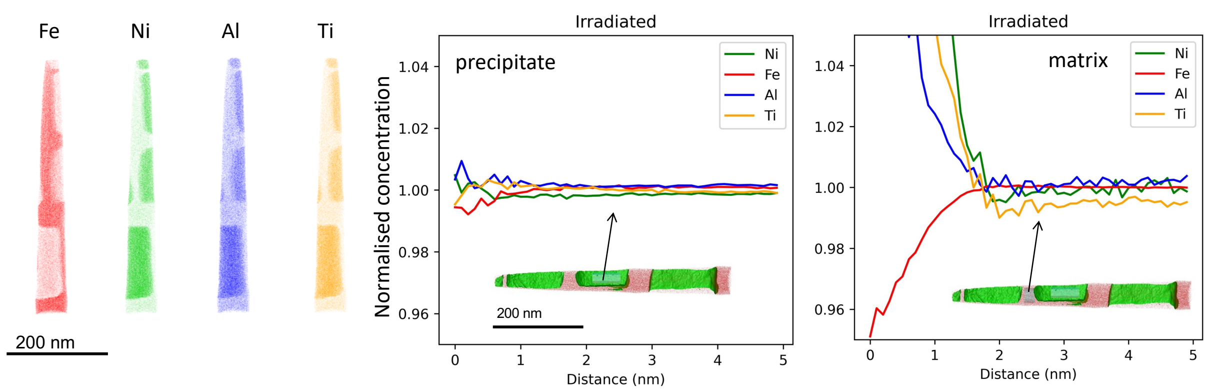

Fig. S10 Element distribution analysis by APT in irradiated FNAT-Fine sample with corresponding element radial distribution function (RDF) analysis in a precipitate and the matrix. The radial distribution function is calculated using the distance between Ni atoms and the others with a pin size of 0.1 nm over 5 nm.

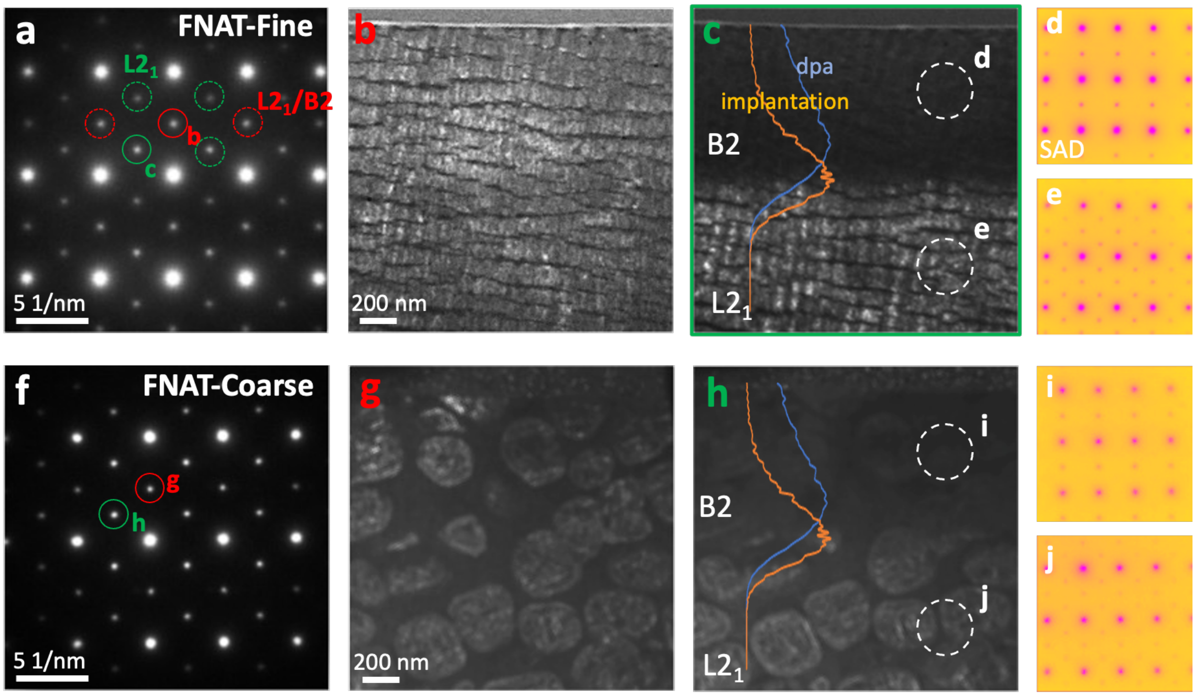

Fig. S11 Radiation induced partial disordering in FNAT-Fine and FNAT-Coarse.

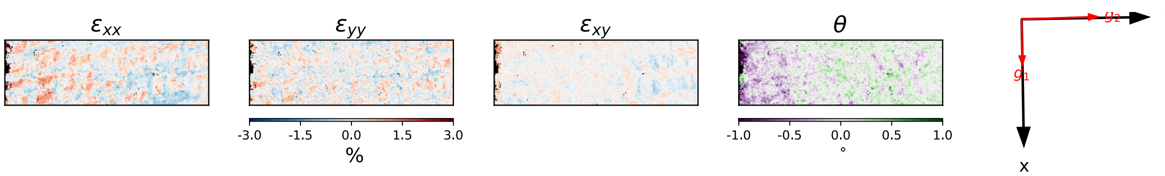

Fig. S12 4D-STEM strain maps in FNAT-Fine irradiated.

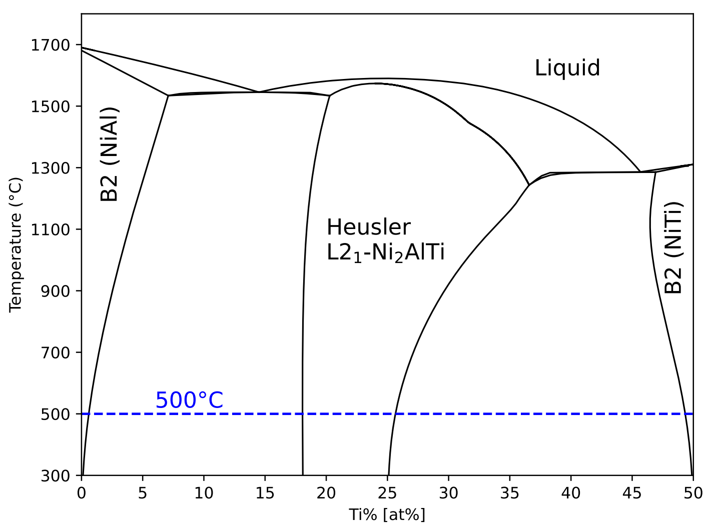

Fig. S13. Pseudo-binary phase diagram of NiAl-NiTi calculated using TCHEA6 database in Thermocalc.

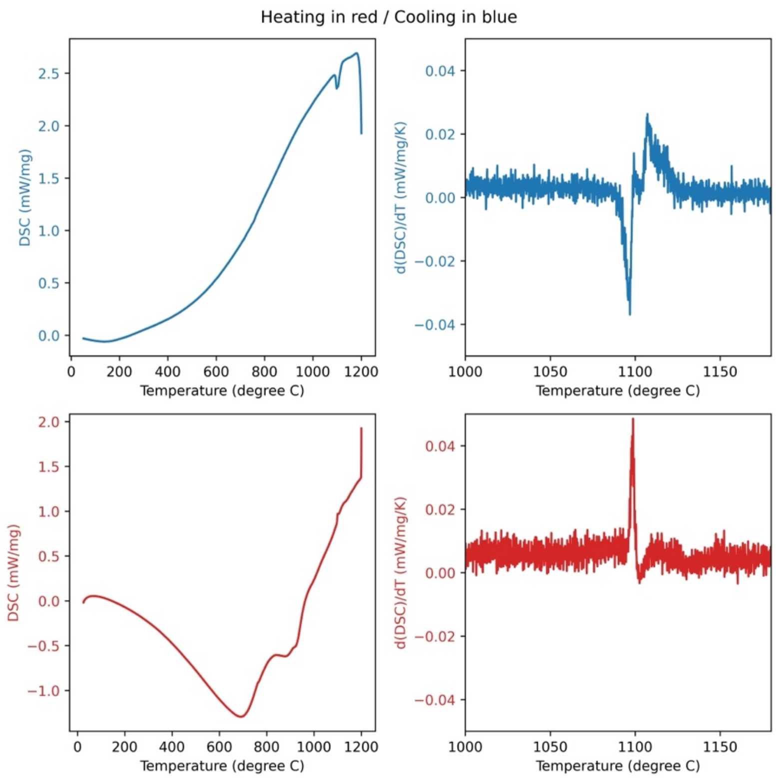

Fig. S14. Differential scanning calorimetry of FNAT alloys from RT to 1200 °C using a NETZSCH STA 449F3 with a heating and cooling rate of 10 K min^{-1}.